Green lithography for delicate materials

Artem K. Grebenko[1,2,†]*, Anton V. Bubis[1,3]*, Konstantin A. Motovilov[2], Viacheslav V. Dremov[2], Evgeny V. Korostylev[2], Ivan L. Kindiak[2], Fedor S. Fedorov[1], Sergey Yu. Luchkin[1], Yuliya V. Zhuikova[4], Aleksandr V. Trofimenko[2], Gleb I. Filkov[2], George V. Sviridov[2], Andrey A. Ivanov[5], Jordan T. Dull[6], Rais N. Mozhchil[3,5], Andrey M. Ionov[3], Valery P. Varlamov[4], Barry P. Rand[6,7], Vitaly Podzorov[8] and Albert G. Nasibulin[1,9,‡]

[1] Skolkovo Institute of Science and Technology, Nobel str. 3, 121205, Moscow, Russia

[2] Moscow Institute of Physics and Technology, Institute Lane 9, 141701, Dolgoprudniy, Moscow District, Russia

[3] Institute of Solid State Physics (RAS), Academician Ossipyan str. 2, 142432, Chernogolovka, Moscow District, Russia

[4] Institute of Bioengineering, Research Center of Biotechnology of the Russian Academy of Sciences, Leninsky Ave.33, bld. 2, 119071, Moscow, Russia

[5] National Research Nuclear University MEPhI (Moscow Engineering Physics Institute), 115409, Moscow, Russia

[6] Department of Electrical Engineering, Princeton University, Princeton, New Jersey 08544, USA

[7] Andlinger Center for Energy and the Environment, Princeton University, Princeton, New Jersey 08544, USA.

[8] Department of Physics and Astronomy, Rutgers University, Piscataway, New Jersey 08854, USA

[9] Aalto University, P.O. Box 16100, FI-00076 Aalto, Finland

* - these authors contributed equally to this work

† - corresponding author, artem.grebenko@skoltech.ru

‡ - corresponding author, a.nasibulin@skoltech.ru

Advances in nanoscience and nanotechnology critically rely on our ability to create electrical contacts to various novel materials[1–7] or modify them at the nanoscale. At the current research frontier, a variety of unconventional materials, including biological nanostructures, organic and hybrid semiconductors, as well as monolayer and other low-dimensional systems, are actively explored. Frequently these materials are poorly compatible with traditional electron beam (e-beam) or deep ultraviolet (DUV) lithographic[8–11] techniques that use harsh organic solvents. Here, we develop a new class of eco-friendly and water soluble lithographic resists based on chitosan, a nature-derived inexpensive material. We describe a physico-chemical principle for achieving truly water-based bottom-up and top-down lithographic approach for the fabrication of nano- and micro-devices based on delicate materials. The proposed technique relies on the unique chelating properties that enable chitosan to be used as a water-based positive tone lift-off e-beam or DUV resist and deliver a resolution down to 100 nm, with a sensitivity of 130 μC/cm^2. As demonstrations of the power of this approach, we have fabricated working μm-scale field-effect transistors (FETs) on individual single-wall carbon nanotubes (SWCNTs) and organic semiconductor (OS) crystals, and we have patterned metal contacts on individual animal's brain microtubules via truly green, water-based lithography for the first time. This work opens an avenue for the investigation of unconventional delicate materials by micro- and nano-device fabrication directly on their surfaces.

Electron beam and deep ultraviolet lithographies (e-beam and DUV, respectively) are among the most reliable micro- and nano-fabrication techniques, delivering device patterning at a high resolution, with a precise match between the design and obtained patterns. However, the conventional implementation of these methods does not permit the fabrication of metal contacts, or any other modification directly on the surface of a wide range of delicate materials. Conjugated organic polymers[1], small-molecule organic semiconductors (OS)[2], biological materials and nanostructures, such as bacterial[3] and artificial peptide[4] nanowires, hybrid perovskites[5], metal-organic frameworks (MOFs)[6], organic self-assembled monolayers (SAMs)[7] and others cannot withstand the chemicals and treatments involved in conventional resist

processing protocols. At the same time, existing solvent-less patterning methods, including imprint nanolithography and hard shadow masks, impose stringent limitations on resolution, lift-off feasibility and require sophisticated fabrication protocols.

There have been several attempts to design e-beam or photo resists based on polyvinyl alcohol (PVA)[8] and CYTOP^{TM}, including combinations of the latter with commercial resists[9,10], which were partially suitable for organic semiconductors. These techniques, however, require baking of the resist films at 150 ^{o}C and additional post-development treatments, such as an oxygen plasma etching, that significantly limit the range of materials compatible with these approaches. One of the most delicate approaches was to utilize water-soluble protective layers, such as dextran or polyacrylic acid, combined with conventional photo lithographic techniques[11]. Unfortunately, these methods provide poor resolution, and more importantly they are not able to deliver a residue-free development, which is the major requirement for further successful processing. In addition, these techniques cannot be extended to e-beam lithography (because of the detrimental crosslinking of protective layers occurring under e-beam), and thus they cannot be used in nanofabrication. One of the first suggested approaches for water-based e-beam and DUV lithographies was to employ a resist made out of fibroin, a protein in a natural silk[12–14]. However, fibroin is naturally insoluble in water, and its processing as a resist relies on strong organic solvents and a complex preparation protocol[15]. Further attempts to develop water-based nanolithography used bio-inspired materials, such as a natural linear polysaccharide pullulan (negative tone)[16], chicken egg albumin (both tones)[17], lysozyme mixture with tris(2-carboxyethyl)phosphine (positive tone)[18] and chitosan (positive tone)[19,20]. Nevertheless, all of these attempts suffered from a common set of problems: (a) the surface of the material of interest within the developed areas of the resist was significantly contaminated with residues; and/or (b) the intact resist removal was impossible without the use of strong acids, plasma etching, or ionic liquids. Therefore, to the best of our knowledge, there are no truly water-based lithography methods capable of a residue free development and a bottom-up fabrication (e.g., the lift-off), necessary for working with delicate materials. We stress again that for the case of a direct bottom-up fabrication on the surface of

delicate materials the issues of resist residues and intact resist removal are extremely important, and successful device fabrication is impossible without solving both of these issues.

The strategy developed in this work is based on chitosan derivatives (CDs), e.g. chitosan salts, serving as the first water soluble, positive-tone resist capable of delivering a reproducible lift-off (bottom-up) and allowing etching (top-down) high-resolution micro- and nano-scale patterns on target substrates. Following the conventional steps of spin-coating and radiation exposure, films of a CD resist are developed in a nearly neutral or acidic aqueous solution of salts of transition-metal (d-block) elements. During the development, unexposed (high molecular weight) areas are protected from dissolution in water by the chelation reaction, while exposed (low molecular weight) ones are dissolved and completely removed (see Methods section and Extended data Fig. **1**). Chelation is a type of bonding between (typically organic) ligands and a metal ion[21]. It should be stressed that for the lithographic principle discussed here, it is not really important which particular irradiation source, transition-metal salt or chitosan derivative are used.

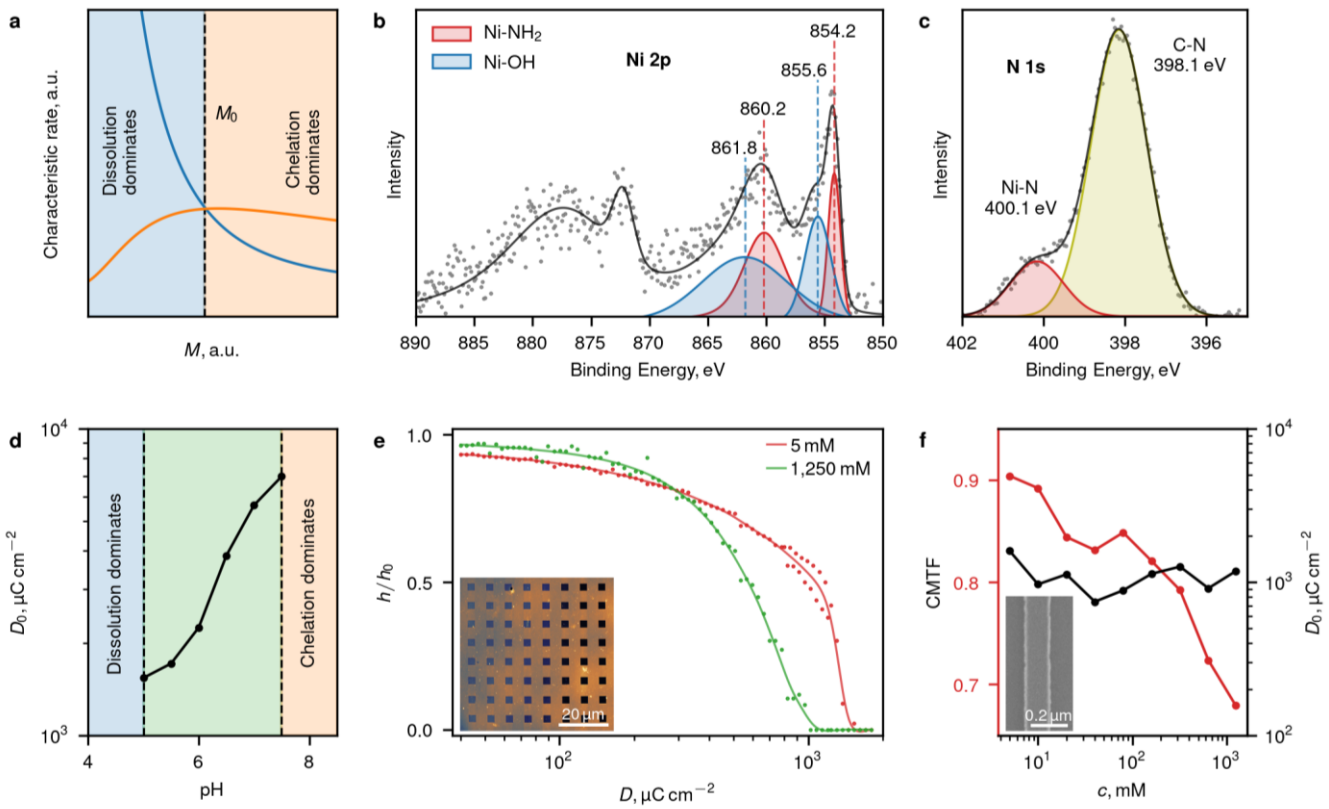

Figure 1. Development of chitosan-based resists. a, Characteristic rates of two competing processes, chelation (orange curve) and dissolution (blue curve) vs molar mass of CD, define the outcome of the development process, where either chelation (faint orange) or dissolution (faint blue) dominates. Ni 2p **(b)** and N 1s **(c)** core level XPS spectra of unexposed chitosan acetate film processed in $NiCl_2$ solution. **d,** The dependence of sensitivity (D_0) on the pH of developer. **e,** Height-dose curves obtained by developing with 5 mM (red curve) and 1,250 mM (green curve) $NiCl_2$ solutions. Inset: AFM image of the sample corresponding to the green curve. **f,** CMTF (red line) decreases with increasing concentration, reaching values typical of conventional resists[28]. The sensitivity (black line), on the other hand, is almost independent of concentration. Inset: individual Ti/Pd line obtained via lift-off using high concentration developer..

Here we focus on the physical and chemical principles of the lithography using a chitosan acetate based resist, an aqueous solution of nickel salts used as a developer, and highly diluted formic acid used as remover (for technical details please refer to Materials and Methods section, while the developer compatibility with other materials is discussed in Supplementary note 1). These data can be used by researchers as a starting point for formulating their own custom-made developers that would meet the requirements of a particular application of interest. We have tested multiple chitosan derivatives, mainly its salts (Extended Data Fig. **2**), to optimize the resist processing. The type of anion and the initial molecular weight of chitosan salts (Extended Data Fig. **3**) mostly affect the hydrodynamic properties of the solution and therefore influence spin coating conditions needed to obtain the required thickness, but they do not affect the development process. We have chosen a chitosan acetate with M = 700 kDa as a representative resist material for electron-beam exposure processing. Below we only discuss aqueous solutions of nearly neutral or acidic nickel chloride and sulphate employed as model developers. However, these can be replaced[21], and we have tested several other transition-metal salts (Extended Data Fig. **4**).The formation of chelate complexes is supported by the X-ray photoelectron spectroscopy (XPS) studies of an unexposed resist film subjected to a 400 mM $NiCl_2$ solution[22]. The Ni 2p (Fig. 1**b**) spectrum is characterized by a spin-orbit doublet (Ni $2p_{3/2}$-$2p_{1/2}$ at 855/872 eV) with satellite structure typical for divalent Ni. A primary Ni $2p_{3/2}$ line at 854.2 eV, followed by a broad satellite peak at 860.2 eV, indicates the formation of Ni-NH_2[23] bonds. Ni-OH bonds are associated with a pronounced shoulder at 855.6 eV and satellite maxima due to multielectron excitation distanced by ca. 6.2 eV[24]. Deconvolution of the N 1s spectrum (Fig. **1c**) reveals two bands with maxima at 398.1 and 400.1 eV, stemming from C-N[25] and Ni-N[23] bonds, respectively. The

additional nitrogen peak in XPS spectra at approximately 400 eV for exposed chitosan was observed after reaction with Ni.

The dissolution of exposed[26] and unexposed[27] chitosan strongly depends on pH of the developer solution, while the chelation rate of Ni[28] is only slightly sensitive to pH. Increasing pH was found to lower the sensitivity D_0, the minimal radiation dose required for a complete removal of the exposed region, as shown in Fig. 1**d**. At a fixed concentration of $NiCl_2$ solution (400 mM) and a set processing time (10 min) chelation reaction dominates for pH > 7.5, preventing the irradiated areas from dissolving for up to the doses of ~10^5 μC/cm^2 (which is already sufficient for carbonization of the resist[29]), while at pH < 5.0, the entire film can be completely dissolved due to the boost in the polymer disentanglement process (see Methods).

Optimization of the transition-metal ion concentration in the developer solution improves the overall height-dose curve steepness, which is demonstrated by the difference between 5 mM (red line) and 1,250 mM (green line) $NiCl_2$ solution used at fixed pH = 5.5 and processing time of 5 min (Fig. 1**e**). The steepness of this curve influences the profile of the developed structures (the wall angle of the resist), which is of critical importance for the subsequent lift-off of the resist. The general trend for the steepness of the height-dose curve to improve is illustrated in Fig. 1**f** in the form of a critical modulation transfer function (CMTF, red line)[30,31] that depends on the developer concentration, while D_0 is practically insensitive to the Ni ion concentration (Fig. 1**f**, black line). Comparison of the development procedures using CMTF = $\frac{D_{100}-D_0}{D_{100}+D_0}$, where D_{100} is the maximum dose leading to no changes in the relative height, is more applicable in our case than conventional contrast $\gamma = \frac{-d(h/h_0)}{dln(D)}|_{D=D0}$ [32,33], due to the high nonlinearity of the height-dose curves in a wide range of concentrations (Extended Data Fig. **5**).

Such a nonlinearity, i.e. the induction effect[32–34], can be rationalized by the influence of water rinsing stage, during which, a fraction of metal ions escape from the surface, and the near-surface region of the resist partially dissolves, resulting in an inhomogeneous distribution of Ni throughout the film thickness captured by XPS (Extended Data Fig. **6**). In the case of high $NiCl_2$ concentrations, the Ni content in the top

layer of the resist is greater, which compensates the loss of Ni ions during rinsing and, respectively, blocks further film dissolution. We found that for a fixed development time of 5 min, $NiCl_2$ concentration greater than 1 M and pH = 5.5, (i.e. CMTF less than 0.7, see Fig. 1**f**) the development yields a reproducible and reliable lift-off with the resolution down to 100 nm. In addition, lower concentrations (5 mM) might be utilized in applications that do not require vertical development profile but demand even gentler processing.

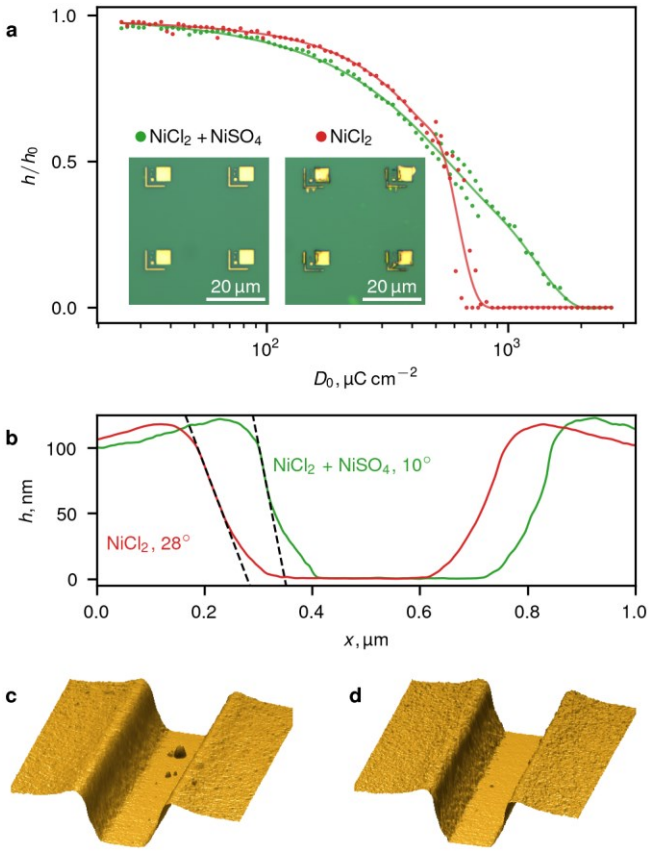

Figure 2. The effect of developer anion. a, The height-dose curves for one-step (red symbols) and two-step (green symbols) development procedures. The inset shows optical microscope images illustrating the difference in the lift-off of the patterned structures. **b,** Representative AFM profiles of developed lines. The two-step development process results in a smaller angle of developed resist walls. **c, d,** A 3D rendering of AFM topography of the lines developed via one-step and two-step development processes, respectively.

The effect of anion is examined by using a $NiSO_4$-based developer. The solutions containing SO_4^{2-} ions yield a development profile suitable for lift-off at concentrations lower than 200 mM, even though a clean surface in a µm-scale range is hard to optimize for this developer (Extended Data Fig. **7**). The concentration of Ni ions within the thickness of the film is notably greater when compared to the chloride solution, as seen from the XPS measurements (Extended Data Fig. **6**), consistent with the earlier report of

the chitosan's sorption capacity[35]. Based on these observations, we formulate one more approach, a two-step development (green line, Fig. **2a**), consisting of consecutive application of $NiCl_2$ and $NiSO_4$ solutions, i.e. salts with low and high sorption capacity. We suggest that high Ni content throughout the resist thickness, ensured through the use of the nickel sulphate, has a major impact on the development profile (see Fig. **2b, c** and **d**) and decrease of the induction effect depicted in Fig. **2a** by the red line, while the chloride solution completely removes the resist residues.

The discussed model solutions reveal that the developer concentration and the type of the anion affect the lift-off process through the improvement of the developed resist wall angle, while the pH of the solution determines the sensitivity. The detailed specific recipes are given in Methods, and their performance is shown in Extended Data **Fig. 8**.

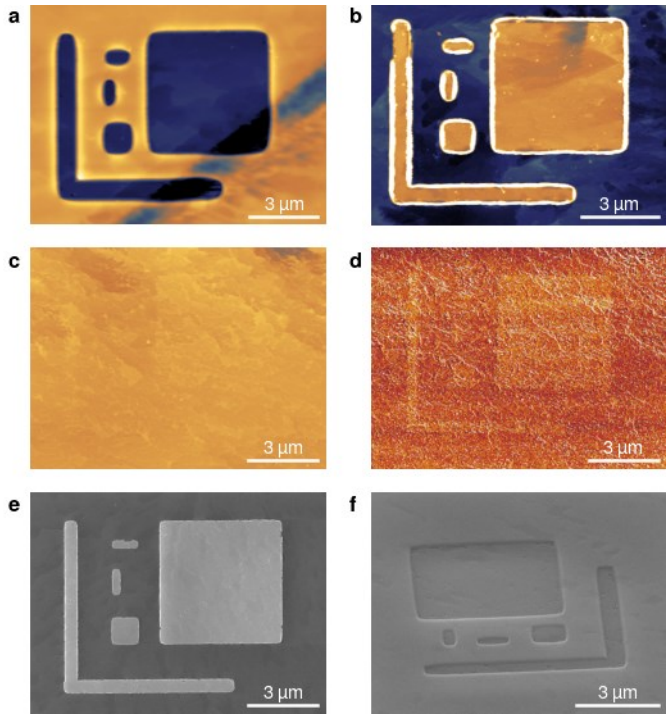

Figure 3. Lithographic patterning directly on the surface of organic semiconductors. a, An AFM image of the developed area in the resist on the surface of a TCNQ crystal. **b,** An AFM image of a similarly processed region of TCNQ crystal after the deposition and lift-off of a Pd film. **c, d,** AFM topography and phase images of the surface of TCNQ single crystals exposed to the same doses as in **a** and **b**. **e, f,** SEM images of lifted-off Pd structures and oxygen plasma etched pattern fabricated on the surface of a rubrene thin film.

To show the extended applicability of the proposed technology, we have employed an e-beam lithographic patterning on the surface of several prototype organic semiconductors. We have successfully

carried out development and lift-off directly on the surface of single-crystalline organic semiconductor tetracyanoquinodimethane (TCNQ)[36] using chitosan based resists (Fig. **3a** and **b**). Well-defined molecular steps, characteristic of organic single-crystal surfaces, can be observed in the developed regions of the resistand under the subsequently evaporated palladium (Pd) layer. Exposure of a bare surface of TCNQ crystals to e-beam at the same dose and the subsequent processing in $NiCl_2$ aqueous solution does not lead to any significant morphological degradation (Fig. **3c**), with only a slight modification of the exposed regions visible in AFM phase scans (Fig. **3d**). We have also performed a successful lift-off patterning of metallic contacts and oxygen plasma etching on the surface of highly crystalline and compact ultra-thin (~20 nm) rubrene films that have macroscopic grain size of up to ~ 0.5 mm grown on polyimide substrates[37,38](Fig. **3e** and **f**). Both organic semiconductors used in this study, as well as many others, are stable[39,40] under the processing conditions during the treatment by the developer and remover solutions (see Supplementary Note **1** for details).

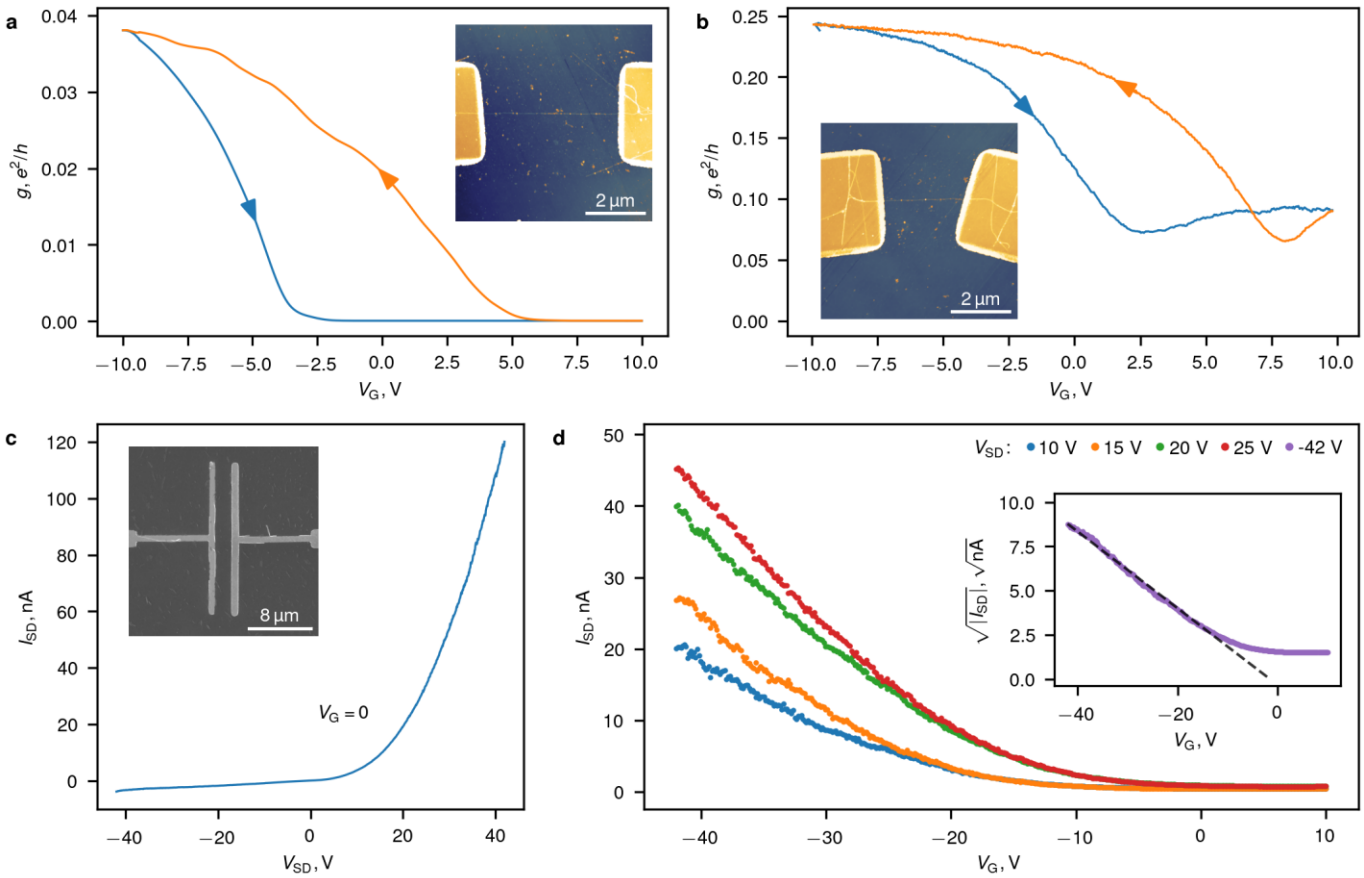

Figure 4. FET devices fabricated directly on delicate materials via water-based chitosan lithography.
a, b, Transconductance characteristics of individual SWCNT FETs demonstrating semiconducting **a** and metallic/semi-metallic **b** behavior. The insets are the false-color AFM images of the corresponding structures. **c,** $I_{SD}(V_{SD})$ at $V_G = 0$ of a polycrystalline rubrene OFET with a 2 μm-long channel, exhibiting a diode-like behavior. Inset: SEM image of the source-drain contact structure. **d,** The transfer $I_{SD}(V_G)$ characteristics of the same OFET in the linear regime. The inset shows a transfer characteristic of the device in the saturation regime.

In order to demonstrate lithographic contact fabrication directly on the surface of delicate materials, we used our water-based lithographic technique and fabricated top-contact field effect transistors (FETs) on very delicate materials: individual single-wall carbon nanotubes and rubrene thin films. In the case of SWCNTs,[41] their small diameter makes this system highly sensitive to resist residue, which makes the lithography process challenging[42] in terms of the cleanliness of developed areas. On the other hand, organic semiconductors are very sensitive to solvents used in the standard semiconductor processing.

For the FET fabrication, we have synthesized SWCNTs by an aerosol (floating catalyst) CVD method[43] and deposited them onto thermally oxidized (300 nm-thick SiO_2) Si wafers (Fig. **4a** and **b**). By performing chitosan-based e-beam lithography, we have obtained 24 individual SWCNT FETs exhibiting transconductance characteristics similar to those reported previously[44] (Fig. **4a** and **b**). More than 60% of the fabricated devices exhibited the ON-state source-drain resistance in the range 10 - 100 kΩ, which is comparable to the devices fabricated with the standard lithographic approaches[45] but has never been reported for a water-based lithography.

Next, we have successfully fabricated several top-contact/bottom-gate organic FETs (OFETs) using the rubrene thin films grown on polyimide substrates[37]. We have intentionally chosen very small channel lengths in the range $L = 0.6$ - 2.2 μm and very narrow metallic electrodes with the width of 0.2 μm in order to demonstrate the potential of this chitosan-based lithography in nano- and micro-structure fabrication (inset in Fig. **4c**). The resultant devices with Pd source and drain contacts show typical diode-like I-V characteristics at zero gate bias (Fig. **4c**) and exhibit FET characteristics with the linear and saturation regime carrier mobilities[46] in the range of $\mu = (2 - 3)\times10^{-3}$ $cm^2V^{-1}s^{-1}$ (Fig. **4d**). These mobilities are lower than those obtained in macroscopic top-gate FETs fabricated on similar polycrystalline rubrene films[37,38]. However, the low mobility of devices fabricated here is not related to the lithography technique that we are

focusing on in this work. The low μ is associated with the top-contact/bottom-gate (staggered) geometry of these FETs, leading to the accumulation channel formed at the bottom of the rubrene film, right at the interface with a 5 nm-thick amorphous tris[4-(5-phenylthiophen-2-yl)-phenyl]amine (TPTPA) seeding underlayer used in these devices for better crystallinity of polycrystalline rubrene films[37]. Additionally, the staggered geometry and Schottky barriers at the Pd/rubrene interface likely lead to a high contact resistance resulting in contact-dominated devices - a problem that is especially severe in the short-channel FETs fabricated here. Nevertheless, we have achieved our current goal of successfully demonstrating a lithographic fabrication of submicron size channels directly on the top surface of organic semiconductors utilizing our novel chitosan-based lithographic approach.

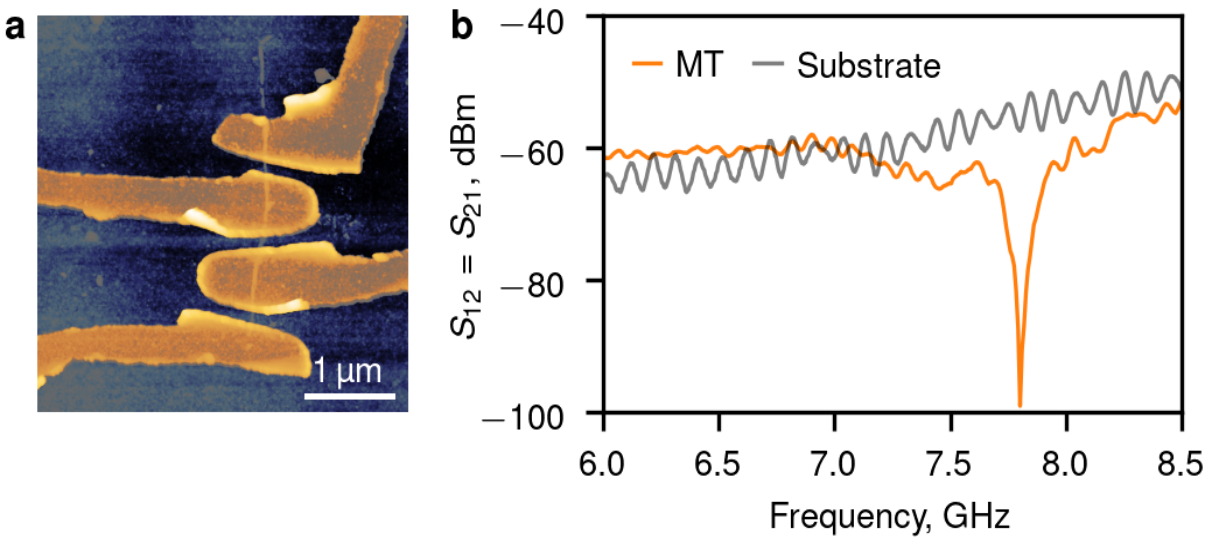

Figure 5. The electric field transmission spectra through an individual porcine brain microtubule. a, An AFM image showing a four-point contact structure lithographically patterned directly on top of the microtubule. **b,** The parameters, S_{12} and S_{21}, of the scattering matrix obtained with VNA, defining the transmission of electric field through the microtubule. Measurements were carried out at 38 °C. Only the high-frequency range, containing one of the resonances relevant to the microtubule, is shown for simplicity. The sample with the microtubule (the orange line) is compared to the same structure but without a microtubule (the grey line).

Finally, we have lithographically defined four-probe contact structures directly on porcine brain microtubules. These contacts are made of … and are separated by 50-100 nm-wide gaps. Thanks to the delicate nature of our truly water-based lithographic approach, there is no damage of the microtubules discernable in AFM imaging, and the devices remain electrically active. We have performed electrical

measurements of these brain microtubules in the frequency range 0 - 8.5 GHz by using an impedance and vector network analyzer (VNA). **Fig. 5** shows the electric-field transmission spectral region of 7-8.5 GHz, where the microtubule shows one of its characteristic resonances, and the signal can be confidently distinguished from the substrate (see Fig. **5** and Extended Data Fig**. 11**). We have observed a narrow (0.08-0.11 GHz) Lorentzian-like electric field absorbance line at 7.2-7.8 GHz in three different samples (the green lines for ambient conditions) that appeared to be sensitive to the external conditions, such as the relative humidity varied between 22% and 95% (the blue lines) and temperature varied between 22°C and ~ 38°C (the orange lines). The observed narrow absorption line[47] can be attributed to the propagation of a kink soliton wave of dipole polarization travelling along the microtubule[48,49], as theoretically predicted earlier by R. Penrose *et al*.[X]. The role of the microscopic surrounding of the microtubule, including bound water at its surface, as well as the effect of temperature, can be described by various models of propagation of such waves[48]. Broadband dielectric response (including GHz range) of biological macromolecules is generally highly sensitive to the level of hydration and temperature. Usually, increasing temperature and an elevated level of hydration both lead to a blue-shift in the observed relaxations[50,51]. In many protein systems, high-temperature charge dynamics is governed by the fundamental frequency-temperature superposition principle clearly demonstrated by corresponding scaling curves[52]. Here, thanks to the proposed lithographic approach, we demonstrate the possibility of fabrication of damage-free, electrically active devices, which opens the avenue for further more detailed investigation of such biological micro- and nano-objects.

To conclude, we have developed a truly water-based positive-tone e-beam and DUV lithographic technique capable of bottom-up (lift-off) approach, where the resist is made out of chitosan derivatives. The proposed technology employs specific chelation chemistry of chitosan and yields a competitive quality of resist development, both in terms of the negligible surface contamination and the developed resist wall's angle. This method is shown to be compatible with the surface of delicate materials, where it results in reliable fabrication of nano- and micro-scale contacts to SWCNTs, organic semiconductors, such as rubrene

and TCNQ, as well as small biological objects - brain microtubules, all of which are incompatible with the conventional wet lithography. The demonstrated water-based lithography opens further opportunities in research, development and applications of micro- and nanostructures based on delicate organic semiconductors, monolayer materials, metal-organic frameworks, biological objects (proteins, DNA, etc.), as well as conjugated polymers. Our technology ensures the complete fabrication routine, including the most frequently used bottom-up processes (lift-off) and top-down (etching), realized directly on the surface of the delicate target materials with a 100 nm resolution. It is a major leap forward in the development of water-based lithography techniques due to the complete development, the possibility of both the bottom-up and the top-down fabrication, and compatibility with a wide range of emergent materials, all demonstrated here for the first time. The employed resist materials and processes are extremely cheap, free from any harsh or toxic chemicals, severe temperature treatments or other aggressive conditions, which makes this technology applicable to a much wider range of materials compared to the modern commercial resists.

References

Online content

Any methods, additional references, Nature Research reporting summaries, source data, extended data, supplementary information, acknowledgements, peer review information; details of author contributions and competing interests; and statements of data and code availability are available at https://doi:xxxx.xxx.x.org

Methods

Chitosan derivatives (Chitosan salts of organic acids)

Chitosan derivatives solutions were prepared in MQ water at the concentration ranging from 1% to 10%. For each particular solution the concentration was tuned to obtain correct thickness at given spinning conditions and substrate size. For the results presented in the main text chitosan acetate (M = 700 kDa) solution was prepared with the concentration of 1.5% wt., spin coated at 2500-3500 rpm, on 5x5 mm^2 substrates, which resulted in the 90-150 nm film depending on the solution age. Chitosan acetate with molecular weight of 700 kDa was synthesized by precipitation purification of the received chitosan sample (Bioprogress LLC, Moscow, Russia) and subsequent titration of 1% acetic acid under rigorous stirring till reaching pH = 4.0 and complete dissolution of the precipitate (complete protonation of chitosan amino groups). See supplementary materials for more details on preparation of the other chitosan derivatives.

Radiation exposure

For DUV experiments we used CL7100 (Optosystems Ltd.) KrF excimer laser with 248 nm wavelength and the laser pulse duration of 20 ns. The energy of the pulse was controlled using LabMax-TOP Laser Power/Energy meter with energy sensor J-50MUV-248. The irradiation was performed at a fluence of 20 mJ/cm^2 per pulse at a repetition rate of 11 Hz for a fixed number of pulses. To form a pattern Al mask on UV-transparent fused quartz was fabricated by the means of e-beam lithography and ICP chlorine etching. Mask was fixed on top of the substrate by a 3D micro-mechanical manipulator for exposure. The approximate dose required for complete development of the exposed region was 1,000 pulses. E-beam lithography was done on Crestec CABL 9000C lithography system. The accelerating voltage was kept constant at 50 kV value. Probe currents varied in range from 50 pA to 10 nA, which led to covered dose range from 25 to 150,000 $\mu C/cm^2$.

Microscopy

Leica DM4500 P LED optical microscope combined with a digital camera was used to analyse the results of the development or lift-off. For more detailed studies of chitosan films morphology, thickness, exposed areas shape, residues quantity, mechanical film properties after various treatments, we used Bruker Multimode V8 Atomic Force Microscope in ScanAsyst-Air, PeakForce-HR and Quantitative NanoMechanical mapping modes. We also utilized Cypher ES microscope (Asylum Research, CA) in tapping mode. Usually soft tips with a spring constant of 0.4 N/m were used. SEM images were obtained at Jeol JSM-7001F at acceleration voltages from 10 to 30 kV.

X-ray Photoelectron spectroscopy

XPS spectra were collected by XPS spectrometer Kratos Axis Ultra DLD with spherical sector analyser, ion gun, ultraviolet and x-ray sources. Experiments were conducted under ultra-high vacuum $5 \cdot 10^{-10}$ - $3 \cdot 10^{-9}$ Torr utilizing the irradiation of AlKα(mono) 1,486.69 eV (energy resolution 0.48 eV, binding energy calibration on Ag $3d_{5/2}$ line and C 1s).

Chelation-dissolution development concept

In classical resist development[34] dissolution rates of the irradiated and pristine resist R_i and R_p are governed by $R_i/R_p = (M_p/M_i)^{\square}$, where $\square$ is the solubility factor and M_i and M_p are the molecular weights of the irradiated and pristine sample, respectively. The solvent, used as a developer, is chosen to increase the solubility factor $\square$, but, at the same time, it is chosen as a weak solvent of a corresponding intact polymer. In order to obtain residue free development we propose to utilize strong solvent for the chitosan derivatives considered in this work — water. This requires an unconventional positive developer that would inhibit dissolution of the unexposed parts of the film in an aqueous developer solution, and to do so, we employ a reaction of chelation of the CD with transition-metal ions[21,53]. The resulting CD chelate complexes are much less soluble in water compared to its pristine form. Irradiation of chitosan and its derivatives with either UV light, x-ray, or electron beam leads to a decrease in molecular weight that depends on the

irradiation dose,[54–57] D: $\frac{1}{M_i} - \frac{1}{M_p} \propto D$. This process is accompanied by a local heating and liberation of gaseous H_2 and NH_3[57] that results in a noticeable thinning of the resist film (Extended data Fig. **9**). The rate of both processes, the dissolution in water and chelation with transition-metal ions, depends on the CD molecular weight. The diffusion lag time[58] τ, of these two reactions can be used to qualitatively distinguish the characteristic time scale of disentanglement responsible for dissolution, τ_{dis}, and the time scale of chelation, τ_{chel}. We consider the processes occurring at the length scale of the polymer's gyration radius, $r_g \propto M^{1/2}$, and thus $\tau \propto \frac{r_g^2}{D_{diff}}$, where D_{diff} is a diffusion coefficient for the particular process. For dissolution, according to the scaling model of polymer disentanglement[59], the coefficient of self-diffusion of a polymer with molecular weight M is $D_{self} \propto \frac{1}{M^2}$, which gives $\tau_{dis} \propto M^3$. In the case of chelation, the model of membrane ion mobility[60] predicts the diffusion coefficient to be $D_{chel} \propto exp\left\{\frac{-1}{M^2}\right\}$ and therefore $\tau_{chel} \propto M\ exp\left\{\frac{1}{M^2}\right\}$. Both of these time constants, $\tau_{dis}$and τ_{chel}, and therefore the respective diffusion rates, $R \propto 1/\tau$, depend on the characteristics of the developer solution that can be tuned to reach the situation depicted in Fig. 1**a**. Two M-dependent characteristic process rates cross at a value M_0, corresponding to the molecular weight below which the dissolution process is faster than the formation of the chelate complex, while for heavier molecules chelation dominates, preserving the high-M regions of the resist. For a particular transition-metal salt developer solution the sharpness of the rate dependencies on M, and the position of M_0 can be varied by the solution pH, concentration of the transition-metal ion or the type of anion.

Developer and remover constituents

$NiCl_2$ (99.9 %) and $NiSO_4$ (99.9 %) were purchased from RusHim company (Moscow, Russia) and used without any additional purification. Herein for all cases of the developer content, aqueous solution of $NiCl_2$ is either nearly neutral or acidic. All reviewed solutions are fully compatible with various possible materials used as a substrate or that form a contact (see Supplementary Note 1). Fresh developer solution was

prepared each time before the experiment. $NiCl_2$ and $NiSO_4$ salts were dissolved in MQ water at a concentration of 5-5,000 mM and their pH was adjusted by HCl and H_2SO_4 to reach the desired value. All developments were carried out in dishes/six-well plates fixed on the orbital shaker working at 200 rpm under 22 °C and RH from 25 to 45 %. For one-step development, the sample was firstly transferred into nickel chloride solution for 5-10 min, afterwards moved to the MQ water on the same orbital shaker for 30 s and finally air dried. For two-step development the first step is 5 min treatment in 200-400 mM $NiCl_2$ water solution with pH = 5.5. Then the chip is transferred into 200-400 mM $NiSO_4$ water solution with pH = 5.5 for additional 5 min. Finally, the chip is rinsed in MQ water for 30 s. As a remover mainly we used highly diluted (0.01-0.1% vol.) formic acid, an eco-friendly food additive, which resulted in fast (ca. 1 min) lift-off and low residues on SiO_2 surface.

To study the development process, a chitosan acetate solution was spin-coated onto commercially available Si wafers with a 300 nm-thick thermal SiO_2. The films were then exposed to a matrix of rectangular test structures (inset in Fig. **1e**) with gradually increasing radiation dose (denoted throughout the text as dose-test pixels). The developed dose-test pixels were studied by an atomic force microscope (AFM), and the height-dose curves were obtained after the processing. We have investigated the dependence of sensitivity, $D_{0,}$ as well as the shape of the height-dose curves on the pH, the concentration and anion type of the transition-metal salt developer solution (see Fig.**1** and Extended Data Fig. **5**).

Optimized lift-off lithography and its performance

After the discussion of development principles, we can formulate two major approaches that can deliver a lift-off capable development (Extended Data Table **1**). The first approach is to utilize a high-concentration developer based on $NiCl_2$ (1 – 5 M solution, at pH 3 – 5, and processing time from 5 to 10 min, followed by 30 s water rinsing), which provides a clean development of the exposed regions (Extended Data Fig. **8a** and Extended Data Fig. **7**), a reproducible lift-off (Extended Data Fig. **8b**), an outstanding 100 nm resolution (Extended Data Fig. **8c** and **d**), and high sensitivity of ca. 130 μC/cm^2. The second recipe targets to lower the chemical reactivity of the developer solution by combining two nickel

salts. This approach enables lowering of the developer concentration down to hundreds of mM at pH ≥ 5.5 (the same processing and rinsing time), while keeping the sensitivity at the order of 1,000 μC/cm^2. Developed and lifted-off structures obtained by the two-step approach are shown in Extended Data Fig. **8e** and **f**. However, the narrowest metal line obtained by two-step development and lift-off is limited to 250 nm (an array of such lines with a 1 μm period is shown in Extended Data Fig. **8g** and **h)**.

Successful realization of the lift-off process also requires a proper solvent to remove the non-exposed film after the deposition of desired material (for instance, metal for contacts). The water itself can be used as a remover, but it might take up to several days to complete the process after chelation. We found that aqueous solutions of weak organic acids, specifically a 0.01-0.1% formic acid solution, is an effective remover, because it provides a rapid film dissolution, clean substrate in the regions previously covered by unexposed film, and it is compatible with a wide range of materials including organic and biological substances, carbon-based nanomaterials and metals. Polymethylmethacrylate (PMMA), one of the most established resist in e-beam lithography, outperforms the proposed here CD based technology in terms of CMTF, contrast and resolution (narrowest individual line obtained via lift-off) when used in accordance with the standard recommended protocol. However, we are able to obtain residue free development, high sensitivity and an outstanding resolution without applying any organic solvents, post development treatments and resist film baking , when compared to earlier reported methods.

Deposition and etching

For deposition of metal films, two evaporation systems were utilized: thermal evaporator Tecuum AG with a base pressure of 1 - 5 · 10^{-6} Torr and electron beam evaporator Angstrom with base pressure of 1 - 5 · 10^{-7} Torr. Plasma etching of OS was performed in Diener Nano plasma generator under 0.3 mbar of oxygen and 200 W source power. We tested Ag, Ti, Cr, Au, Sn, Au, Al, Pd thermal and e-beam deposition on tetracyanoquinodimethane (TCNQ) to examine the adhesion to the surface, needed to withstand the removal of the non-exposed chitosan acetate film during the lift-off. The best results are illustrated in Extended Data Fig. **10.** All other metals listed above but not shown in the figure demonstrated worse

adhesion and detachment of the metallic pattern during resist removal. Palladium (Pd) was a metal of choice for its good adhesion to rubrene and TCNQ.

OS synthesis

Single crystals of rubrene and TCNQ[61] were grown by physical vapor transport in a stream of ultra-high-purity helium gas. The materials were purchased at Sigma Aldrich. Temperatures in the sublimation zone during the crystal growth were kept around 320 and 280 °C for rubrene and TCNQ, respectively. The temperature gradient along the growth tube was ~ 5 °Ccm^{-1}, and the helium flow rate was 150 sccm. These materials, typically van der Waals molecular crystals, are characterized by delicate surfaces prone to thermal or chemical degradation via formation of defects either due to sublimation of surface molecules, their fast dissolution in organic solvents or as a result of their interaction with the ambient environment. Such sensitivity makes many organic semiconductors largely incompatible with conventional lithographic processing. For this reason, contact structures are usually first prepared on Si/SiO2 wafers or other substrates, followed by deposition of organic semiconductor films. This approach, however, has a number of limitations, and direct deposition of high-resolution (lithographically defined) contacts on the surface of organic semiconductor is highly desirable.

For the fabrication of polycrystalline rubrene thin films, Si/polyimide substrates coated with ITO, aluminum oxide (100 nm) and tris[4-(5-phenylthiophen-2-yl)-phenyl]amine (TPTPA) (5 nm) were prepared by following the previously published procedure[37]. Rubrene (sublimed grade, Nichem, USA) was deposited by thermal evaporation (20 nm), followed by annealing on a hot plate at 140 °C for 6 min in a nitrogen atmosphere.

FET Fabrication

Several individual SWCNTs and their small bundles were identified and located by using an AFM relative to markers. The rest of the tubes were etched away by oxygen plasma, keeping chosen SWCNTs covered by the resist. We have then spin-coated chitosan acetate and performed e-beam lithography followed by the

two-step development, with the subsequent deposition of Ti (5 Å) and Pd (15 nm) contacts via e-beam evaporation. For the case of OFETs we similarly performed two-step development chitosan-based lithography with subsequent deposition of 12 nm Pd layer and lift-off. For all cases lift-off was performed by 0.1 % formic acid aqueous solution.

Brain microtube patterning

99% pure porcine brain pre-formed microtubules MT-002-A (Cytoskeleton, USA) were resuspended according to the protocol in 15 mM HEPES buffer (pH = 7.0) with 1 mM $MgCl_2$ and 30 µl of 2 mM paclitaxel solution in DMSO. Afterwards, Si/SiO_2 (300 nm SiO_2 thickness) substrates with landmarks were processed in oxygen plasma and covered with the solution containing microtubules, left for 15 minutes, thoroughly washed with MQ water and air dried. Microtubules were localized relative to the landmarks with the help of an AFM operating in PeakForce tapping regime with a fixed load at 1-2.5 nN. Chitosan acetate resist based e-beam lithography was performed, utilizing two-step development approach. Cr (1 nm)/Pd (24 nm) contacts were thermally evaporated, and the chip was subjected to the lift-off procedure in 0.1% formic acid solution.

Electrical measurements

Measurements of OFETs' characteristics were performed under ambient conditions with a Keysight B1500A Semiconductor Analyser equipped with two high rate source-measure units and a probe station. For measurements in vacuum (below $4x10^{-5}$ Torr), the sample holders were wire-bonded with Al wire on a home-built chipholder system connected to a BNC output. SWCNT-FETs were measured with the help of MFLI lock-in and 10^8 A/V transimpedance amplifier connected to Bruker Nanoscope V controller ADC. Four-probe microtubule devices were investigated with the help of B1500A Semiconductor Analyzer (DC measurements), MFIA Impedance analyzer (frequency range from 1 Hz to 5 MHz) and NI-5632 Vector Network Analyzer (frequency range from 300 kHz to 8.5 GHz). For all data obtained with VNA, 0 dBm input power was used.

Data availability

All data underlying this study are available from the https://doi.org/10.6084/m9.figshare.12120903 (https://figshare.com/s/a239d3d91bcad106e007)

Acknowledgments

The development concept was designed under financial support by Russian Science Foundation under grant 19-73-10154. The experiments of the model developer investigation were supported by Russian Science Foundation under grant No. 18-72-10135. XPS was carried out with the support of the Research Facility Center at the Institute of Solid State Physics (RAS) (R.N.M. and A.M.I). This work was performed using equipment of MIPT Shared Facilities Center. F.S.F. acknowledge Russian Fund for Basic Research for the support of spin-coating and ellipsometry tests, grant no. 19-07-00300. F.S.F and A.G.N. thank the Academy of Finland for Mobility Grant (application number 333620). This work was also supported by Skoltech NGP Program (Skoltech-MIT joint project). V.P. acknowledges support from the National Science Foundation under the grant ECCS-1806363. B.P.R. and J.T.D. acknowledge support from the National Science Foundation Award No. ECCS- 1709222. Section on the synthesis of chitosan acetate with various molecular weights was supported by Ministry of Science and Higher Education of the Russian Federation. A.A. I. expresses gratitude to the Russian Foundation for Basic Research (project no. 19-29-03021 mk) for supporting his work. A.G.N and A.K.G. acknowledge RFBR grant 19-32-90143

Author contributions

A.K.G. and A.V.B. performed all experiments on lithography, developer design and lift-off, K.A.M. and V.V.D. formulated ideas of chelation inhibition of the dissolution, E.V.K. consulted on e-beam and photolithography and fabricated masks for DUV experiments, F.S.F. performed ellipsometry experiments

and made interpretation of XPS data, S.Yu.L. made AFM measurements of OSC, Y.V.Zh. and V.P.V. synthesized chitosan acetate samples with various molecular weights, A.V.T., G.I.F. and G.V.S synthesized all other chitosan derivatives, A.A.I. performed DUV exposure experiments, J.T.D. and B.P.R. fabricated thin-film rubrene samples, R.N.M. and A.M.I. performed XPS analysis of the samples, V.P. synthesized single-crystal organic semiconductors, I.L.K. performed VNA measurements of individual microtubules, A.G.N, V.P., A.K.G., A.V.B. and F.S.F. wrote the manuscript. All others commented on the manuscript.

Competing interests

Authors declare no competing interests.

References

1. Xu, Y., Zhang, F. & Feng, X. Patterning of Conjugated Polymers for Organic Optoelectronic Devices. *Small* **7**, 1338–1360 (2011).
2. Pron, A. & Rannou, P. Processible conjugated polymers: from organic semiconductors to organic metals and superconductors. *Prog. Polym. Sci.* **27**, 135–190 (2002).
3. El-Naggar, M. Y. *et al.* Electrical transport along bacterial nanowires from Shewanella oneidensis MR-1. *Proc. Natl. Acad. Sci.* **107**, 18127–18131 (2010).
4. Amit, M. & Ashkenasy, N. Electronic Properties of Amyloid β-Based Peptide Filaments with Different Non-Natural Heterocyclic Side Chains. *Isr. J. Chem.* **54**, 703–707 (2014).
5. Harwell, J. *et al.* Patterning Multicolor Hybrid Perovskite Films via Top-Down Lithography. *ACS Nano* **13**, 3823–3829 (2019).
6. Falcaro, P., Buso, D., Hill, A. J. & Doherty, C. M. Patterning Techniques for Metal Organic Frameworks. *Adv. Mater.* **24**, 3153–3168 (2012).
7. Casalini, S., Bortolotti, C. A., Leonardi, F. & Biscarini, F. Self-assembled monolayers in organic electronics. *Chem. Soc. Rev.* **46**, 40–71 (2017).
8. Park, J. *et al.* Direct top–down fabrication of nanoscale electrodes for organic semiconductors using fluoropolymer resists. *Appl. Phys. A* **111**, 1051–1056 (2013).
9. Jang, J. *et al.* The development of fluorous photolithographic materials and their applications to achieve flexible organic electronic devices. *Flex. Print. Electron.* **1**, 023001 (2016).
10. Ismail, A. G. Photolithographically patterned N-channel organic thin film transistors using sensitized polyvinyl alcohol. *Org. Electron.* **56**, 111–115 (2018).
11. Linder, V., Gates, B. D., Ryan, D., Parviz, B. A. & Whitesides, G. M. Water-Soluble Sacrificial Layers for Surface Micromachining. *Small* **1**, 730–736 (2005).
12. Kim, S. *et al.* All-water-based electron-beam lithography using silk as a resist. *Nat. Nanotechnol.* **9**,

306–310 (2014).

13. Sun, Y.-L. *et al.* Aqueous multiphoton lithography with multifunctional silk-centred bio-resists. *Nat. Commun.* **6**, 1–10 (2015).

14. Park, J. *et al.* Eco-friendly photolithography using water-developable pure silk fibroin. *RSC Adv.* **6**, 39330–39334 (2016).

15. Wang, H., Zhang, Y., Shao, H. & Hu, X. A study on the flow stability of regenerated silk fibroin aqueous solution. *Int. J. Biol. Macromol.* **36**, 66–70 (2005).

16. Takei, S. *et al.* Application of natural linear polysaccharide to green resist polymers for electron beam and extreme-ultraviolet lithography. *Jpn. J. Appl. Phys.* **53**, 116505 (2014).

17. Jiang, B. *et al.* Water-Based Photo- and Electron-Beam Lithography Using Egg White as a Resist. *Adv. Mater. Interfaces* **4**, 1601223 (2017).

18. Wang, D. *et al.* 2D Protein Supramolecular Nanofilm with Exceptionally Large Area and Emergent Functions. *Adv. Mater.* **28**, 7414–7423 (2016).

19. Voznesenskiy, S. S., Nepomnyaschiy, A. & Kulchin, Y. N. Study of Biopolymer Chitosan as Resist for Submicron Electronic Lithography. *Solid State Phenomena* https://www.scientific.net/SSP.213.180 (2014) doi:10.4028/www.scientific.net/SSP.213.180.

20. Caillau, M. *et al.* Fifty nanometer lines patterned into silica using water developable chitosan bioresist and electron beam lithography. *J. Vac. Sci. Technol. B* **35**, 06GE01 (2017).

21. Pestov, A. & Bratskaya, S. Chitosan and Its Derivatives as Highly Efficient Polymer Ligands. *Molecules* **21**, 330 (2016).

22. Yang, F., Liu, H., Qu, J. & Paul Chen, J. Preparation and characterization of chitosan encapsulated Sargassum sp. biosorbent for nickel ions sorption. *Bioresour. Technol.* **102**, 2821–2828 (2011).

23. Matienzo, J., Yin, L. I., Grim, S. O. & Swartz, W. E. X-ray photoelectron spectroscopy of nickel compounds. *Inorg. Chem.* **12**, 2762–2769 (1973).

24. McIntyre, N. S. & Cook, M. G. X-ray photoelectron studies on some oxides and hydroxides of

cobalt, nickel, and copper. *Anal. Chem.* **47**, 2208–2213 (1975).

25. Vieira, R. S., Oliveira, M. L. M., Guibal, E., Rodríguez-Castellón, E. & Beppu, M. M. Copper, mercury and chromium adsorption on natural and crosslinked chitosan films: An XPS investigation of mechanism. *Colloids Surf. Physicochem. Eng. Asp.* **374**, 108–114 (2011).

26. Li, J., Du, Y. & Liang, H. Low molecular weight water-soluble chitosans: Preparation with the aid of cellulase, characterization, and solubility. *J. Appl. Polym. Sci.* **102**, 1098–1105 (2006).

27. Koev, S. T. *et al.* Chitosan: an integrative biomaterial for lab-on-a-chip devices. *Lab. Chip* **10**, 3026–3042 (2010).

28. Pradhan, S., Shukla, S. S. & Dorris, K. L. Removal of nickel from aqueous solutions using crab shells. *J. Hazard. Mater.* **125**, 201–204 (2005).

29. Duan, H. *et al.* Sub-10-nm half-pitch electron-beam lithography by using poly(methyl methacrylate) as a negative resist. *J. Vac. Sci. Technol. B* **28**, C6C58-C6C62 (2010).

30. Bowden, M. J. The Physics and Chemistry of the Lithographic Process. *J. Electrochem. Soc.* **128**, 195C (1981).

31. Tai, K. L. *et al.* Submicron optical lithography using an inorganic resist/polymer bilevel scheme. *J. Vac. Sci. Technol.* **17**, 1169–1176 (1980).

32. Brunner, T. A. Relationship between the slope of the HD curve and the fundamental resist process contrast. *J. Vac. Sci. Technol. B Microelectron. Nanometer Struct. Process. Meas. Phenom.* **17**, 3362–3366 (1999).

33. Cattoni, A. *et al.* Sub-10nm electron and helium ion beam lithography using a recently developed alumina resist. *Microelectron. Eng.* **193**, 18–22 (2018).

34. Moreau, W. M. Developing Resist Images. in *Semiconductor Lithography: Principles, Practices, and Materials* (ed. Moreau, W. M.) 459–544 (Springer US, 1988). doi:10.1007/978-1-4613-0885-0_10.

35. Mende, M., Schwarz, D., Steinbach, C., Boldt, R. & Schwarz, S. The Influence of Salt Anions on Heavy Metal Ion Adsorption on the Example of Nickel. *Materials* **11**, 373 (2018).

36. Menard, E. *et al.* High-Performance n- and p-Type Single-Crystal Organic Transistors with Free-Space Gate Dielectrics. *Adv. Mater.* **16**, 2097–2101 (2004).

37. Fusella, M. A. *et al.* Use of an Underlayer for Large Area Crystallization of Rubrene Thin Films. *Chem. Mater.* **29**, 6666–6673 (2017).

38. Choi, H. H. *et al.* Hall Effect in Polycrystalline Organic Semiconductors: The Effect of Grain Boundaries. *Adv. Funct. Mater.* **n/a**, 1903617.

39. Maricle, D. L. & Maurer, Arthur. Pre-annihilation Electrochemiluminescence of Rubrene. *J. Am. Chem. Soc.* **89**, 188–189 (1967).

40. Ballester, L. *et al.* Hexaazamacrocyclic Nickel and Copper Complexes and their Reactivity with Tetracyanoquinodimethane. *Inorg. Chem.* **46**, 3946–3955 (2007).

41. Iijima, S. & Ichihashi, T. Single-shell carbon nanotubes of 1-nm diameter. *Nature* **363**, 603–605 (1993).

42. Goldoni, A., Larciprete, R., Petaccia, L. & Lizzit, S. Single-Wall Carbon Nanotube Interaction with Gases: Sample Contaminants and Environmental Monitoring. *J. Am. Chem. Soc.* **125**, 11329–11333 (2003).

43. Moisala, A. *et al.* Single-walled carbon nanotube synthesis using ferrocene and iron pentacarbonyl in a laminar flow reactor. *Chem. Eng. Sci.* **61**, 4393–4402 (2006).

44. Laird, E. A. *et al.* Quantum transport in carbon nanotubes. *Rev. Mod. Phys.* **87**, 703–764 (2015).

45. Piatrusha, S. U. *et al.* Noise Insights into Electronic Transport. *JETP Lett.* **108**, 71–83 (2018).

46. Choi, H. H., Cho, K., Frisbie, C. D., Sirringhaus, H. & Podzorov, V. Critical assessment of charge mobility extraction in FETs. *Nat. Mater.* **17**, 2–7 (2018).

47. Havelka, D., Cifra, M. & Kučera, O. Multi-mode electro-mechanical vibrations of a microtubule: In silico demonstration of electric pulse moving along a microtubule. *Appl. Phys. Lett.* **104**, 243702 (2014).

48. Satarić, M. V., Tuszyński, J. A. & Žakula, R. B. Kinklike excitations as an energy-transfer mechanism in microtubules. *Phys. Rev. E* **48**, 589–597 (1993).

49. Mańka, R. & Ogrodnik, B. A model of soliton transport along microtubules. *J. Biol. Phys.* **18**, 185–189 (1991).

50. Kent, M. & Meyer, W. Complex permittivity spectra of protein powders as a function of temperature and hydration. *J. Phys. Appl. Phys.* **17**, 1687 (1984).

51. Grebenko, A. *et al.* Impedance spectroscopy of single bacterial nanofilament reveals water-mediated charge transfer. *PLOS ONE* **13**, e0191289 (2018).

52. Motovilov, K. A. *et al.* Observation of dielectric universalities in albumin, cytochrome C and Shewanella oneidensis MR-1 extracellular matrix. *Sci. Rep.* **7**, 15731 (2017).

53. El-Rehim, H. A. A., Zahran, D. A., El-Sawy, N. M., Hegazy, E.-S. A. & Elbarbary, A. M. Gamma irradiated chitosan and its derivatives as antioxidants for minced chicken. *Biosci. Biotechnol. Biochem.* **79**, 997–1004 (2015).

54. Yoksan, R., Akashi, M., Biramontri, S. & Chirachanchai, S. Hydrophobic Chain Conjugation at Hydroxyl Group onto γ-Ray Irradiated Chitosan. *Biomacromolecules* **2**, 1038–1044 (2001).

55. Sionkowska, A. *et al.* Thermal and mechanical properties of UV irradiated collagen/chitosan thin films. *Polym. Degrad. Stab.* **91**, 3026–3032 (2006).

56. Chmielewski, A. G. Chitosan and radiation chemistry. *Radiat. Phys. Chem.* **79**, 272–275 (2010).

57. García, M. A. *et al.* Effect of molecular weight reduction by gamma irradiation on the antioxidant capacity of chitosan from lobster shells. *J. Radiat. Res. Appl. Sci.* **8**, 190–200 (2015).

58. Ash, R. & Barrie, J. A. Time lag in diffusion. *J. Appl. Polym. Sci.* **31**, 1209–1218 (1986).

59. Miller-Chou, B. A. & Koenig, J. L. A review of polymer dissolution. in (2003). doi:10.1016/S0079-6700(03)00045-5.

60. Peppas, N. A. & Meadows, D. L. Macromolecular structure and solute diffusion in membranes: An overview of recent theories. *J. Membr. Sci.* **16**, 361–377 (1983).

61. Podzorov, V. Organic single crystals: Addressing the fundamentals of organic electronics. *MRS Bull.* **38**, 15–24 (2013).

62. Derjaguin, B. V., Muller, V. M. & Toporov, Yu. P. Effect of contact deformations on the adhesion of particles. *J. Colloid Interface Sci.* **53**, 314–326 (1975).

63. Zainol, I., Md Akil, H. & Mastor, A. Effect of γ-irradiation on the physical and mechanical properties of chitosan powder. *Mater. Sci. Eng. C* **29**, 292–297 (2009).

Extended Data

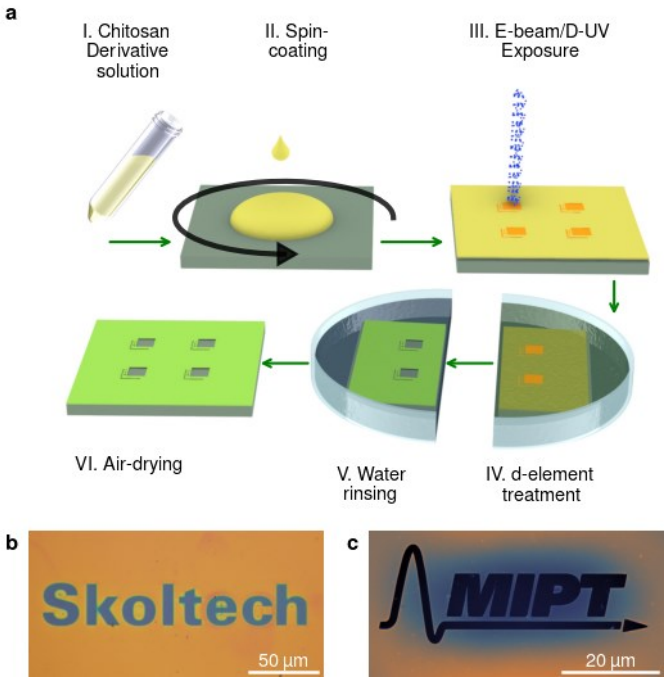

Extended Data Figure 1. Chitosan based lithography. a, A step-by-step procedure for using a chitosan derivative (CD) as a positive-tone resist for lithography. First, an aqueous solution of CD (I) is spin-coated onto the target substrate/material (II). The resulting film is then exposed to either e-beam or DUV radiation (III). The development process consists of a treatment with an aqueous solution of one or two transition-metal salts (IV), followed by rinsing in water (V) and air drying (VI). **b,** An optical microscope image of a logo patterned in a film of chitosan formate (165 kDa) by an excimer 248 nm laser through an Al mask. **c,** An atomic-force microscopy image (topography) of a logo patterned in chitosan acetate (65 kDa) film by e-beam.

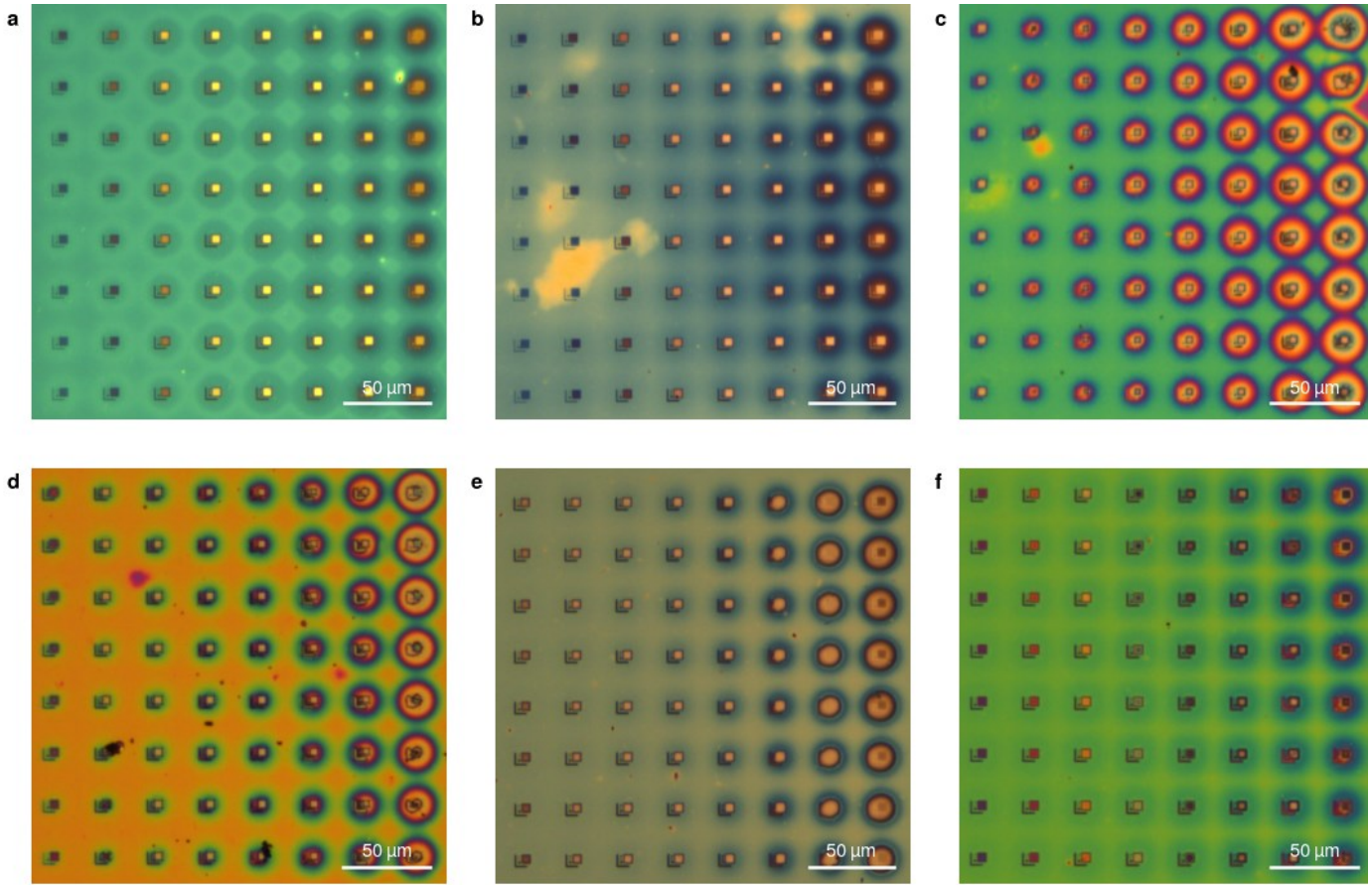

Extended Data Figure 2. Chitosan derivatives subjected to regular dose-test pixels. Optical microscope images of the exposed and developed dose-test pixels from 500 to 15,000 µC/cm^2. All derivatives were dissolved in distilled water and spin-coated on the surface of Si/SiO_2. $NiCl_2$ development: c = 400 mM, pH = 5.5, and development time of 10 min was employed for all cases. The sensitivity for each derivative lies in the range 1000-3500 µC/cm^2. **(a)** Chitosan acetate, **(b)** chitosan formate, **(c)** chitosan glycolate, **(d)** chitosan lactate, **(e)** chitosan succinate, **(f)** carboxymethyl chitosan.

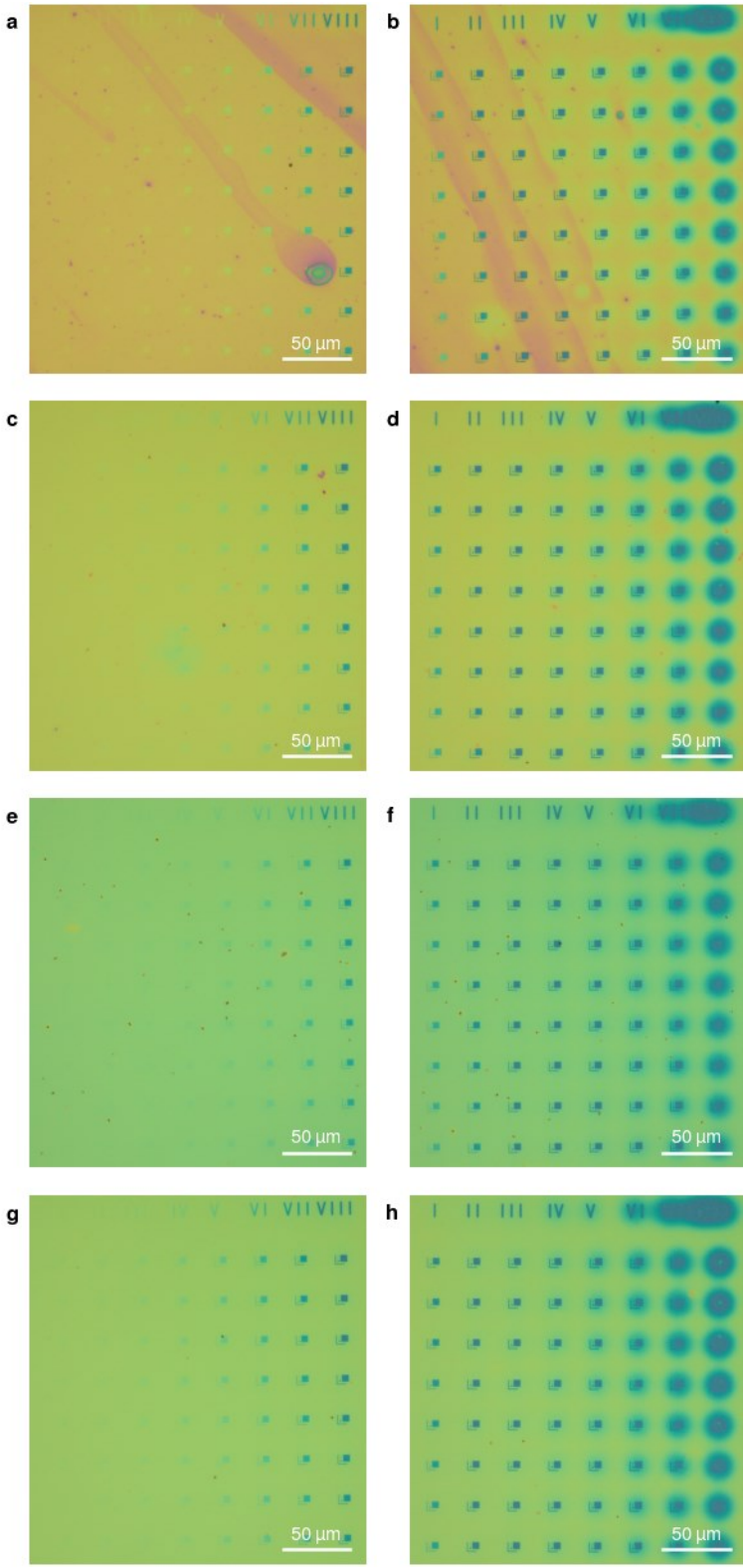

Extended Data Figure 3. Various molecular weights of CD. Optical microscope images showing developed structures in the chitosan acetate film with an exponentially increasing radiation dose. Left column corresponds to the dose range from 25 to 750 µC/cm^2, right column to the dose range from 500 to 15,000 µC/cm^2. **a, b,** 20 kDa; **c, d,** 65 kDa; **e, f,** 200 kDa; **g, h,** 700 kDa. The film thicknesses were fixed at 90 nm. For all the cases two-step development was used.

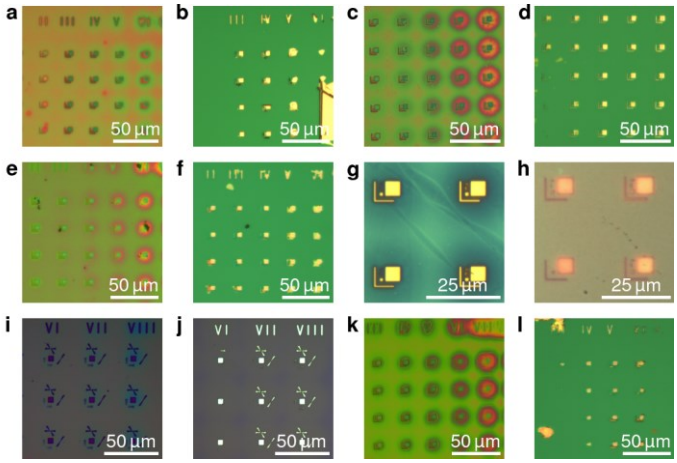

Extended Data Figure 4. Developers based on transition element salts. Optical microscope images of development and subsequent metallization and lift-off of the regions of dose-test pixels. Development salts are **(a, b)** nickel chloride 200 mM, 5.7 pH; **(c, d)** nickel sulfate 200 mM, 5.0 pH; **(e, f)** Mohr's salt 200 mM, 4.1 pH; **(g, h)** cobalt acetate 450 mM, 5.5 pH; **(i, j)** silver nitrate 400 mM, 5.5 pH; **(k, i)** copper sulfate 200 mM, 3.7 pH.

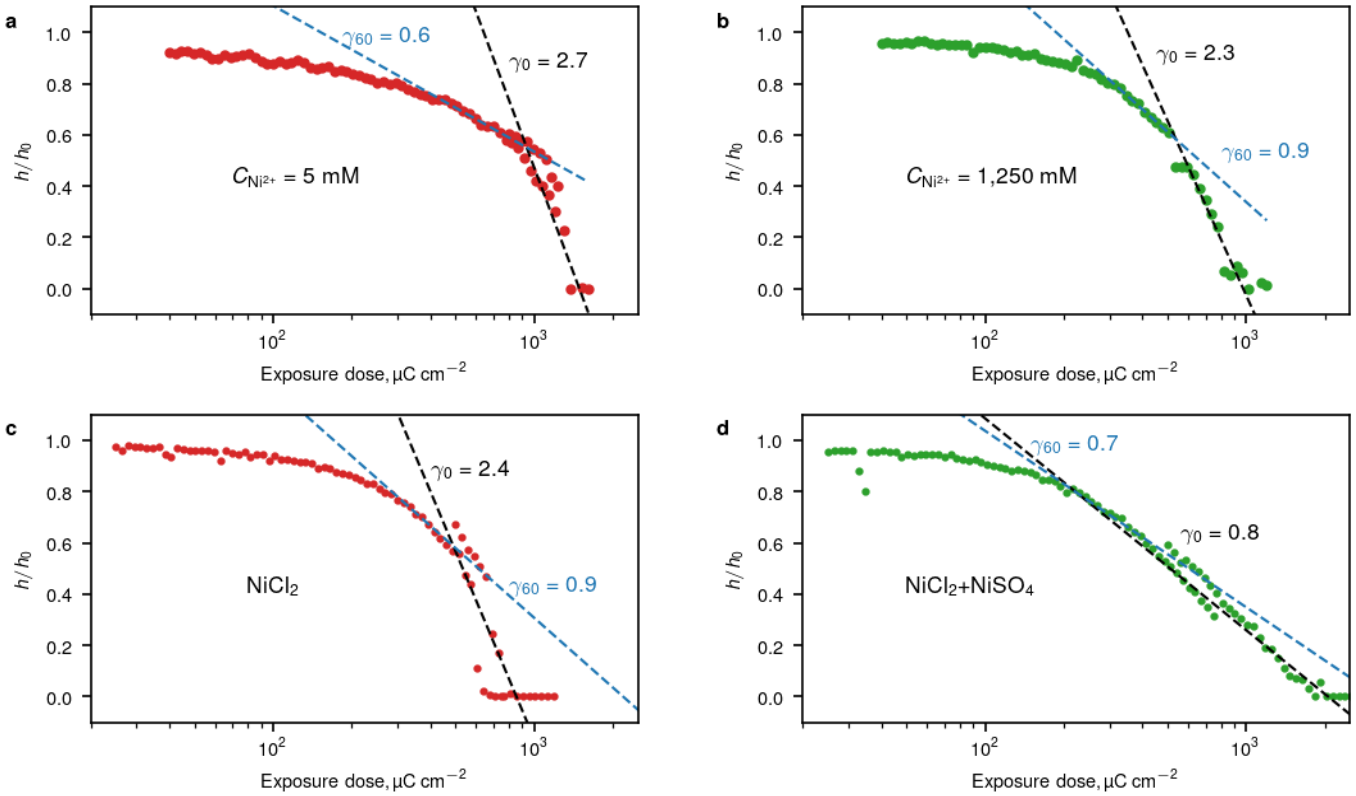

Extended Data Figure 5. Height-dose curves at different concentrations and using different development approaches. **a, b,** The improvement of the height-dose curve steepness due to the concentration increase from 5 to 1,250 mM. **c, d,** The comparison of the one and two-step development approaches. Black dashed line is a slope of the curve to cross the sensitivity D_0, and blue dotted lines touch the curve at 60% of the residual height.

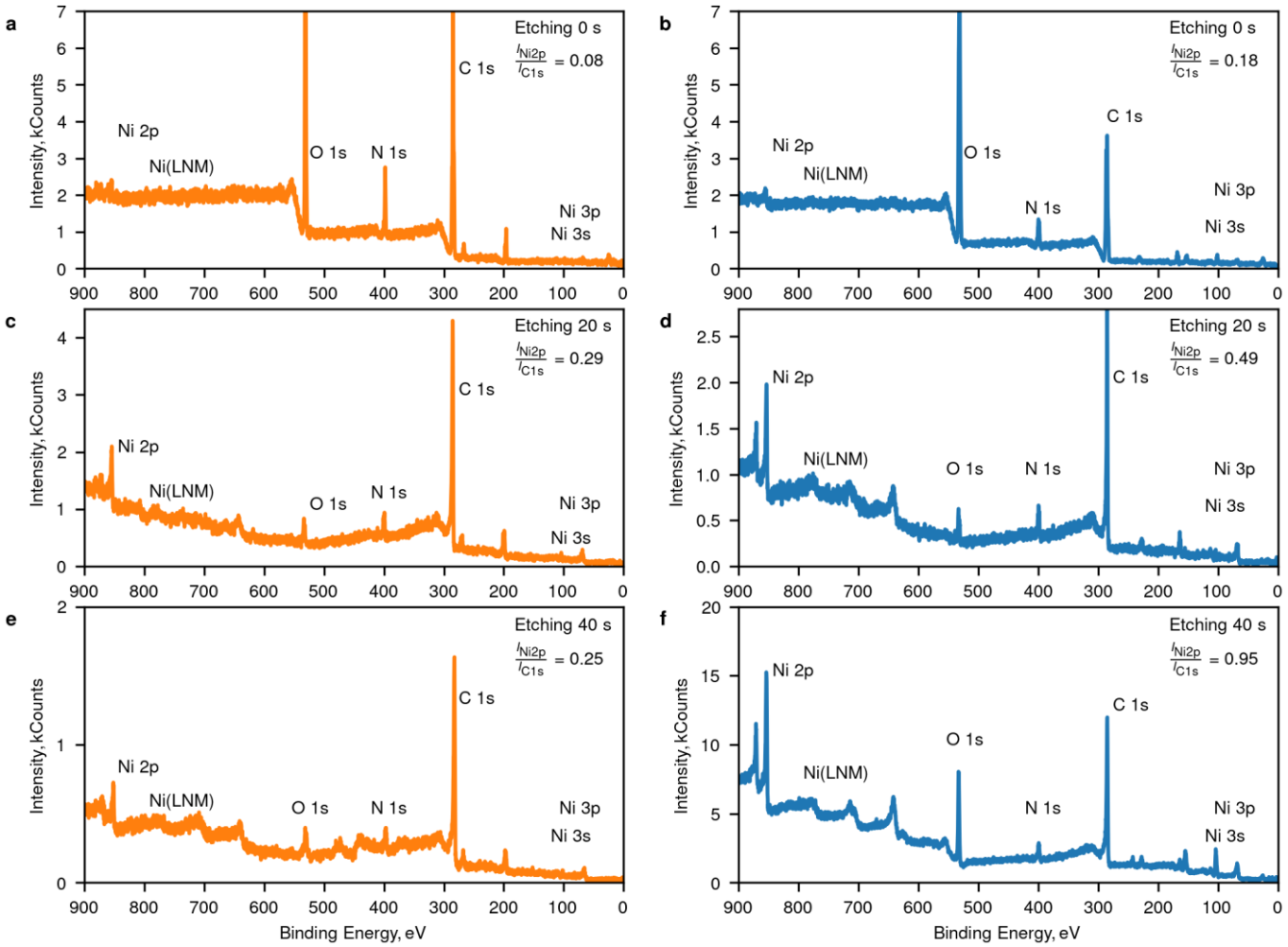

Extended Data Figure 6. XPS data of chitosan acetate films processed with Ni cation solutions. a, 700 kDa film subjected to $NiCl_2$ (400 mM, pH = 5.5, 10 min). **c, e,** the same film after 20 and 40 s of Ar etching, respectively. **b, d, f,** Data obtained in similar conditions for $NiSO_4$ treatment (400 mM, pH = 5.5, 10 min).

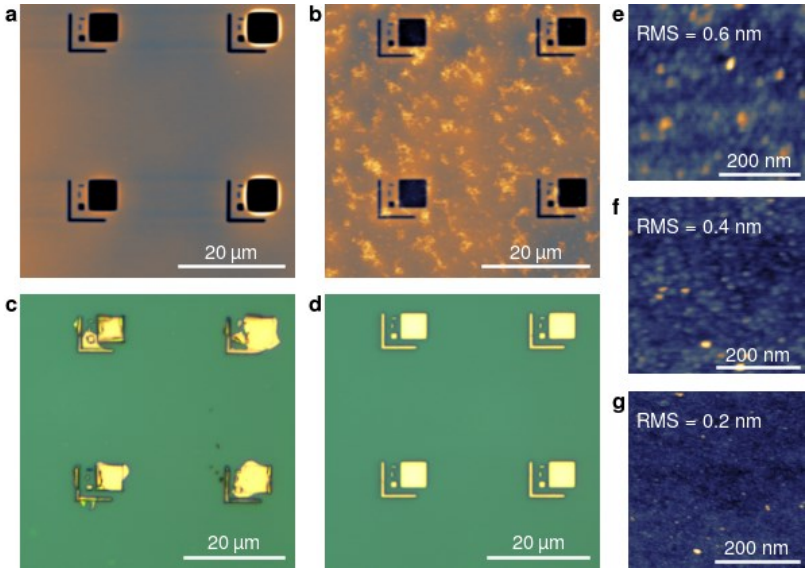

Extended Data Figure 7. $NiCl_2$ vs $NiSO_4$ development. a, AFM image of the developed areas in chitosan acetate film after 400 mM $NiCl_2$ solution processed for 10 min. **b,** AFM image of the same dose-test pixels region developed by $NiSO_4$ solution. The resist residues and modification of the film surface can be clearly seen in **b**. **c, d,** Optical microscope images of Ti/Au structures obtained by means of lift-off. **c,** film was developed by 400 mM $NiCl_2$ 10 min and **(d)** two-step development was used. **e, f, g,** AFM images of the developed areas in the resist depending on the development time of 1, 5 and 10 min, respectively (for one-step development by 400 mM $NiCl_2$ solution at pH = 5.5). The substrate (Si/SiO_2) RMS is roughly 0.2 nm.

Extended Data Table 1. Comparison of the chitosan lithography introduced in this work with the commercial PMMA and other lift-off capable soft methods for e-beam lithography. D_0 is the sensitivity, the accelerating voltage is indicated in brackets, post-development are additional treatments of the developed areas required for development completion, CMTF is the critical modulation transfer function, PMMA 950K A4 and A6 are the commercial resists based on polymethylmethacrylate, CYTOP™ is the fluoropolymer used as a gate insulator and e-beam resist, ZEP520 is a commercial e-beam and D-UV resist. S is a solvent of a resist, D is its developer solution and R is a solvent used for resist removal. Resolution is the narrowest individual line obtained via lift-off.

Properties	**One-step 5 M pH= 3.5**	**Two-step 200 mM pH=5.5**	PMMA 950k A4[43]	PMMA 950k A6 no bake[44]	CYTOP and ZEP520 used for OS FETs[8]
D_0, μC/cm^2	**130 (50 kV)**	**2,000 – 4,000 (50 kV)**	~250 (50 kV)	2,300 (≥100 kV)	~200 (30 kV)
Post-development	**-**	**-**	-	-	Oxygen plasma etching
Baking	**-**	**-**	150-180 ℃	Pump overnight	180 ℃
Solvents	**S: H_2O D: $NiCl_2$ in H_2O R: 0.1 % HCOOH in H_2O**		S: Anisole D: MIBK+IPA R: NMP/Acetone		S: Anisole/FC-40 D: hexyl acetate + FC-40 R: PF-5060
CMTF	**0.5**	**0.7**	0.1 – 0.2	-	-
Contrast (γ)	**3**	**1**	6 – 9	-	-
Resolution, nm	**100**	**250**	10	<500	100

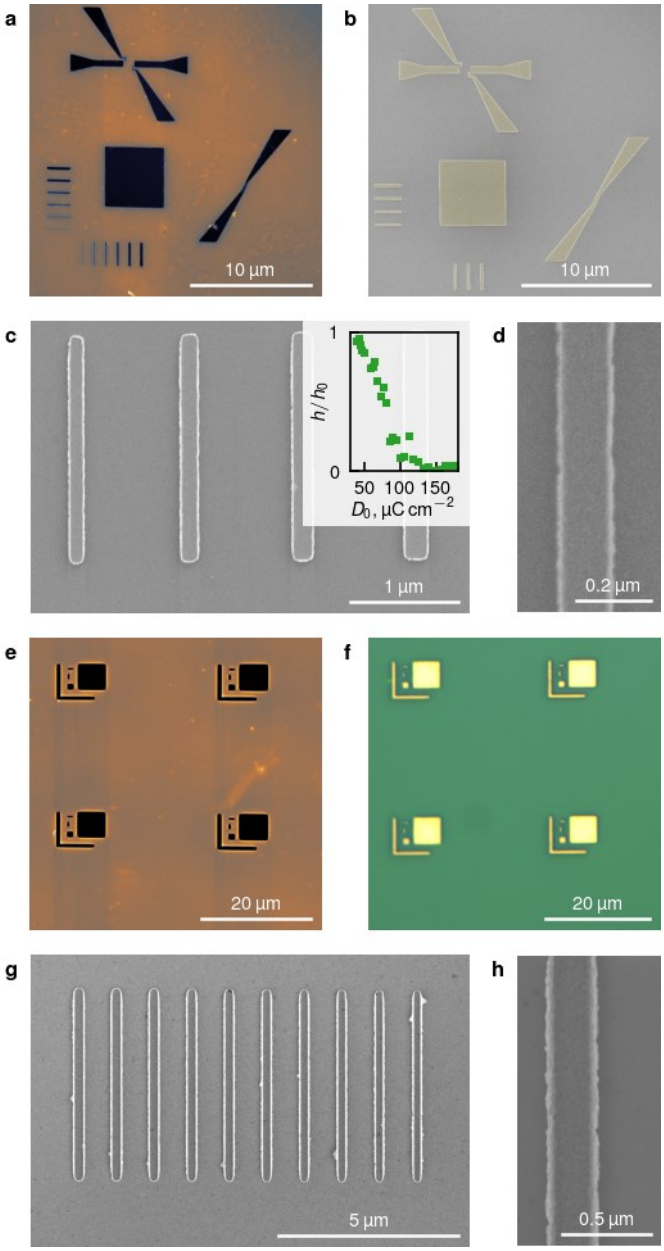

Extended Data Figure 8. Examples of micro- and nano-structures fabricated via chitosan lithography. a, AFM and **b, c, d,** SEM images of the developed and lifted-off structures processed with a high-concentration developer (5 M, pH = 4.0, $NiCl_2$ solution, for 5 min), demonstrating a resolution of ca. 100 nm. The thicknesses of the developed resist and deposited metal films were 70 and 19 nm, respectively. On the inset of the panel **c** height-dose curve for one-step development is shown. **e, f,** AFM and optical microscope images of the developed and lifted-off array of dose-test pixels structures (developer: 400 mM solutions of $NiCl_2$ and $NiSO_4$ in water with pH = 5.5, applied sequentially for 5 min each, followed by a 30 s rinse in water) with the smallest feature size of 300 nm. **g**, **h,** SEM images of critical-dimension structures formed by the two-step developer: 250 nm-wide lines with 1 µm period. In the case of two-step development, the resist thickness was 110 nm, and the metal coating consisted of Ti (1 nm) and Au (19 nm) deposited prior to lift-off.

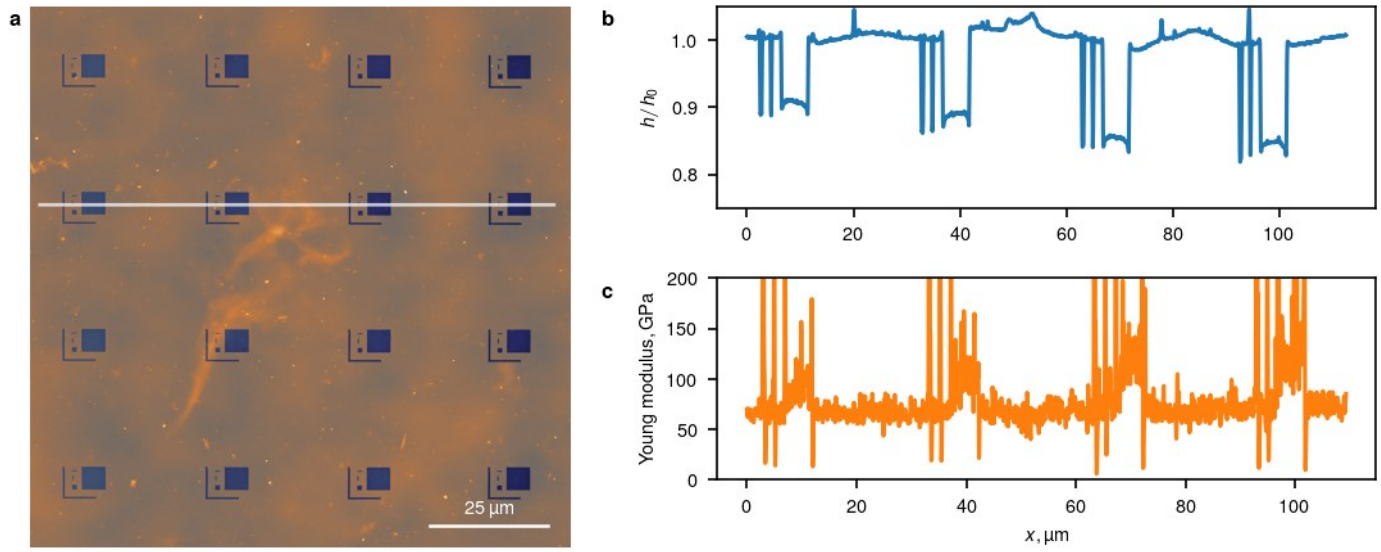

Extended Data Figure 9. Quantitative nano-mechanical AFM maps of exposed but not developed regions of chitosan acetate film. a, AFM topography image of a part of the dose-test pixels structure. **b,** AFM height profile taken along thin white line in panel **a** illustrating the relative remaining thickness. **c,** Young modulus[62] profile taken along the same line of the scan. Liberation of gas molecules and decrease of the molecular weight result both in morphological change[57] (volume decrease depicted in **a**) and increase of Young modulus[63] in **b**. All these data support the model of depolymerization occuring in the regions exposed to the radiation.

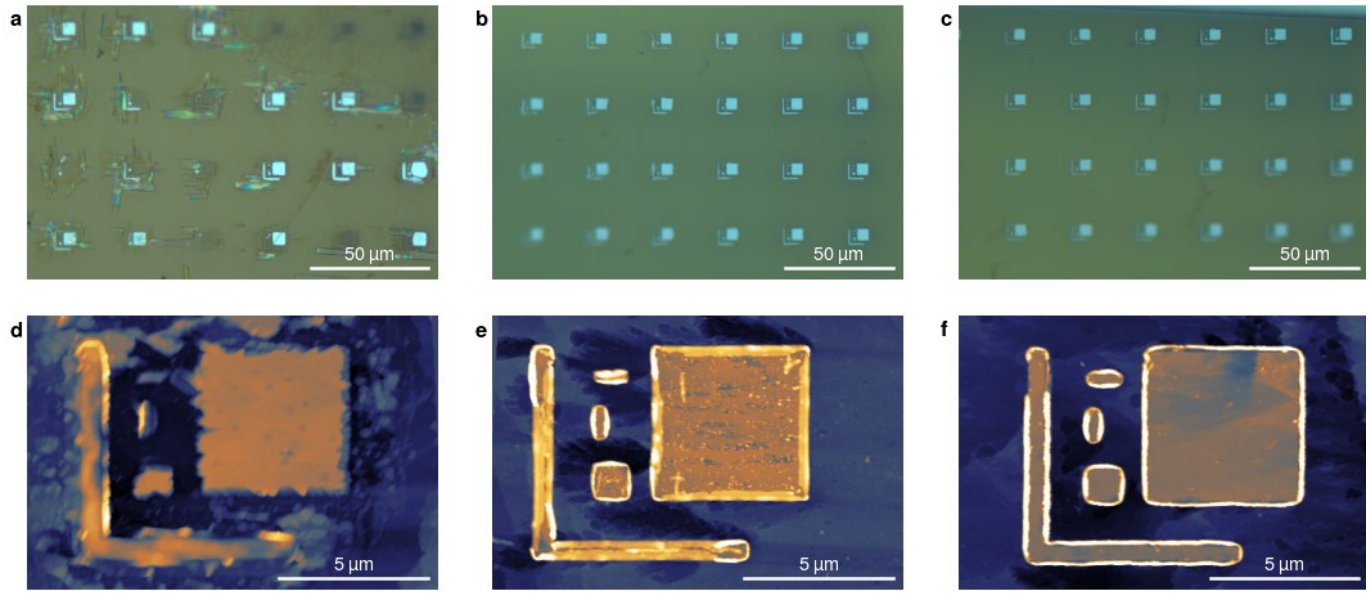

Extended Data Figure 10. Metal deposition on the surface of tetracyanoquinodimethane (TCNQ). a, b, c, Photographs of the lifted-off structures formed by the chitosan based lithography on the surface of TCNQ after deposition of Al (12 nm), Ti/Pd (0.5/12 nm) and Pd (12 nm), respectively. **d, e, f,** Corresponding AFM images of the individual elements of the dose-test pixels. Pure palladium keeps the surface integrity and provides reliable adhesion for lift-off of the sub-micron metallic features on the surface of organic semiconductors.

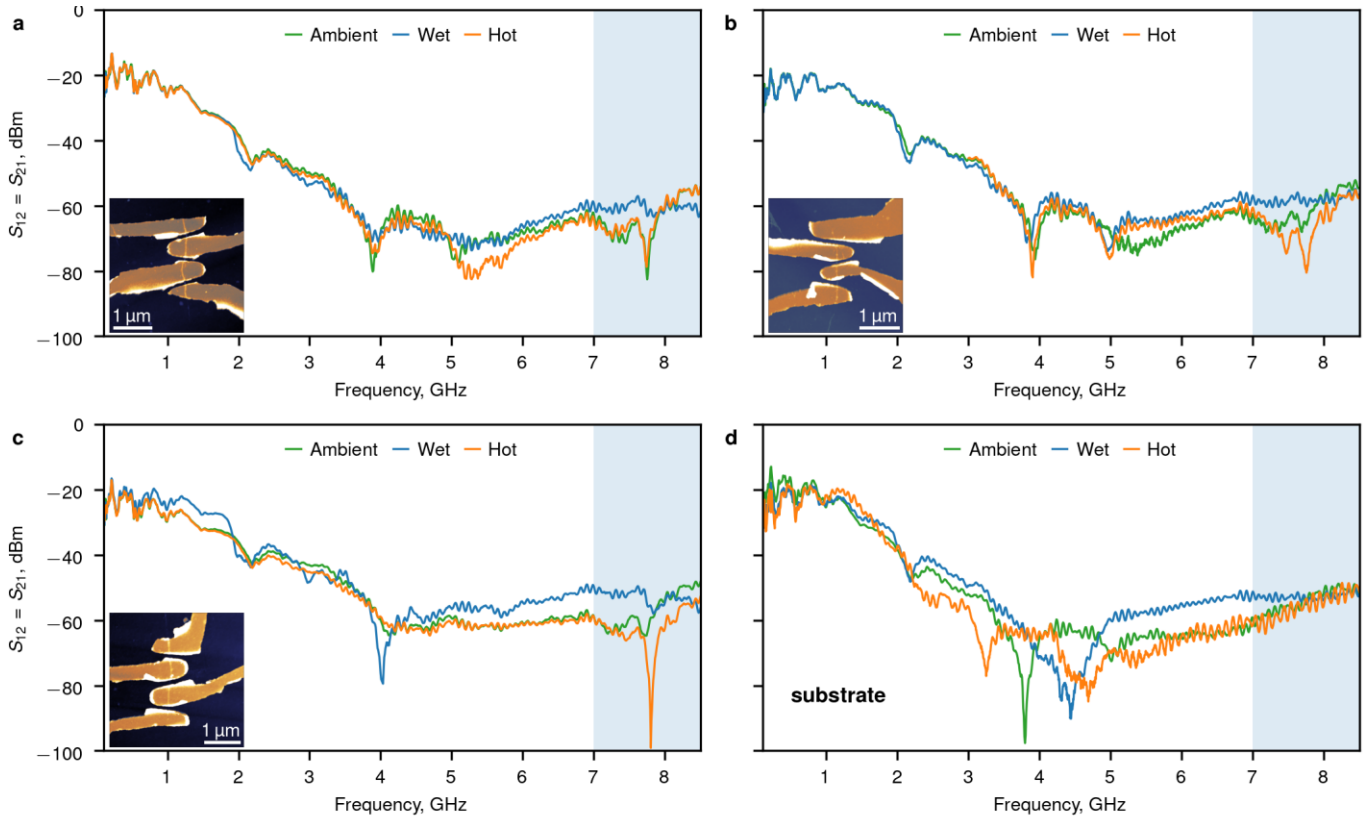

Extended Data Figure 11. Electrical field transmission of individual porcine brain microtubule. a, b, c Electrical field transmission through individual porcine brain microtubule with Pd contacts patterned by chitosan lithography approach. Minimal intercontact gap is 48 nm. Absorbance of the electrical field at ~ 7.5 GHz senses the change of the surrounding medium and can be clearly distinguished from the substrate. **d** Electrical field transmission of the same substrate on top of which samples **(a-c)** were fabricated.